Neuropsychologia 221 (2026) 109322

Contents lists available at ScienceDirect

Neuropsychologia

journal homepage: www.elsevier.com/locate/neuropsychologia

Seeing through the static: Reduced imagery vividness in aphantasia is associated with impaired temporal lobe signal complexity

Chanelle Noble [a,b], Natasha L. Taylor [a,c], Fraser Milton [d], Jon Fulford [e], Joshua B. Tan [a], Claire O'Callaghan [a], Adam Zeman [f], James M. Shine [a,b,*]

[a] Brain and Mind Centre, The University of Sydney, Sydney, NSW, Australia
[b] Centre for Complex Systems, School of Physics, The University of Sydney, Sydney, NSW, Australia
[c] Central Clinical School, Faculty of Medicine and Health, The University of Sydney, Sydney, NSW, Australia
[d] Department of Psychology, University of Exeter, Exeter, EX4 4QG, UK
[e] Department of Medical Imaging, University of Exeter, Exeter, EX1 2LU, UK
[f] Centre for Clinical Brain Sciences, University of Edinburgh, Edinburgh, UK

ARTICLE INFO

Keywords:
Aphantasia
Hyperphantasia
Mental Imagery
Neuroimaging
Vividness
Connectivity
Information
Complexity

ABSTRACT

Aphantasia is the inability to experience mental imagery during full wakefulness without any prominent perceptual deficits. Visual aphantasia is associated with differences in distributed brain networks, but its neurobiological underpinnings remain a mystery. In particular, aphantasia may arise due to impairments in the top-down control over visual imagination. We predicted that this in turn would prevent the brains of aphantasic participants from differentiating neural activity encoding the contents of imagination from the background noise of resting activity, particularly within the ventral temporal lobes. To test this hypothesis, we re-analysed functional magnetic resonance imaging (fMRI) data collected from aphantasics ($n = 21$), hyperphantasics (those with "photographic imagery"; $n = 20$), and controls ($n = 17$) during a simple perception and imagery task. We used two measures of informational complexity to quantify the complexity of the spatial pattern of thresholded BOLD signals in the participants' temporal lobes during visual perception and imagery. Both measures of spatial complexity showed significant correlations with imagery vividness. We then performed dynamic functional connectivity analyses on the same data revealing that the higher-order networks of aphantasics were abnormally coupled with the temporal lobes during imagery ($p < 0.05$). These results provide a novel perspective, reframing aphantasia as an inability of the visual system to selectively activate regions encoding object-specific visual categories above background levels of noise.

1. Introduction

Our subjective visual experiences arise both in the presence and absence of overt retinal stimulation, with the latter referred to as mental imagery. The vividness of mental imagery – or the degree to which imagined visual experiences resemble veridical perception – varies substantially across individuals. A subset of the population (approximately 4 %) with *aphantasia* reports the total absence of imagery during wakefulness (Dance et al., 2022; Zeman, 2024; Zeman et al., 2010, 2015). It remains poorly understood as to why visual aphantasics experience reduced imagery vividness while having broadly intact perceptual abilities, especially when we consider that the networks for perception and imagery overlap in the ventral temporal lobes (Ishai et al., 2000; Lee et al., 2012; Liu et al., 2025; Mechelli et al., 2004; Milton et al., 2021; Spagna et al., 2021).

While the current study focuses on visual aphantasia, it is important to note it has been argued that 'aphantasia' should also refer to individuals with minimal experience of imagery involving other sensory modalities (e.g., auditory, kinaesthetic, etc.; Dawes et al., 2023; Monzel et al., 2022). Aphantasics experience substantially normal perception, and are able to perform tasks we typically associate with imagery (perhaps using different cognitive strategies); most even report visual dreams (Dawes et al., 2020; Keogh et al., 2021; Zeman et al., 2010, 2015). Given the subjective nature of imagery, the possibility has been

This article is part of a special issue entitled: Aphantasia published in Neuropsychologia.

* Corresponding author. The University of Sydney, NSW, 2006, Australia.
E-mail address: mac.shine@sydney.edu.au (J.M. Shine).

https://doi.org/10.1016/j.neuropsychologia.2025.109322
Received 16 May 2025; Received in revised form 13 November 2025; Accepted 17 November 2025
Available online 20 November 2025

raised that aphantasia is due to a lack of meta-cognitive awareness (for discussion, see Zeman, 2024). However, several experiments have provided objective corroboration for the subjective reports of people with visual aphantasia (Kay et al., 2022; Keogh and Pearson, 2018, 2024; Purkart et al., 2025; Wicken et al., 2021).

Popular theories of how the visual system supports imagery describe the process as resembling perception, albeit in reverse (Pearson, 2019). As such, research has typically focused on the primary visual cortices as being the site most essential for processing visual information to generate imagery. But recent evidence suggests that there is activity in the primary visual cortices of aphantasics that can be dissociated from subjective visual experience (Cabbai et al., 2024; Milton, 2024). Others have even argued that the primary visual cortices are not essential for imagery generation at all, and that higher-order visual regions are necessary instead (Cabbai et al., 2024; Milton, 2024). For instance, regions in the ventral temporal lobes, such as the parahippocampal place area (PPA) and fusiform face area (FFA), encode object-specific visual categories (Ishai et al., 2002; O'Craven and Kanwisher, 2000). Activity decoded from these regions during perceptual tasks can be used to successfully decode imagery contents above chance, suggesting similar patterns of activation during perception and imagery (Horikawa and Kamitani, 2017; VanRullen and Reddy, 2019). Furthermore, it is generally agreed upon that imagery generation involves input from frontoparietal regions which is fed-forward and processed in the ventral temporal lobes (Dijkstra et al., 2018, 2019, 2020; Fulford et al., 2018; Mantegna et al., 2025; Pearson, 2019; Spagna et al., 2021, 2024; Winlove et al., 2018). Interestingly, recent 7 Tesla (T) functional magnetic resonance imaging (fMRI) evidence shows a putative imagery hub in the fusiform gyrus of the ventral temporal lobes that is functionally decoupled from frontoparietal networks in aphantasics during imagery attempts (Liu et al., 2025). We therefore rationalised that the ventral temporal lobes are a promising site for identifying a neural correlate of reduced imagery vividness in aphantasia.

If this is the case, then how might information be processed differently in the brains of individuals with aphantasia? One possibility is suggested by evidence from Keogh et al. (2020), who found that imagery vividness is anticorrelated with visual cortex excitability. This could mean imagery vividness may be determined by how well the brain can selectively activate specific subsets of neurons above some threshold relative to background activity – i.e. by the signal-to-noise ratio in visual processing regions. Keogh et al. investigated excitability-related effects in the primary visual cortices, likely because they used transcranial direct-current stimulation and were limited to accessible regions; however, it is possible a similar mechanism also occurs in the ventral temporal lobes of aphantasics. If aphantasics have impaired top-down control over cortical activity in the ventral temporal lobes, then inhibitory modulatory feedback connections in these regions would not sufficiently suppress background activity, preventing specific, differentiated patterns of activity during imagery, while bottom-up sensory input during perception would be precise enough to generate specific population codes (Huang et al., 2017; Hupé et al., 1998; Pace et al., 2023). By way of analogy, if we envisage the resting brain as akin to the visual static we see on a non-tuned television channel, an individual with typical imagery should be able to voluntarily "tune" this static to a particular image (akin to finding a coherent image on a specific station), whereas an aphantasic would be incapable of this process, only being able to modulate the strength of activity overall and hence, rendering their brain dynamics – during imagination – as indistinguishable from a static, white noise process.

To test this hypothesis, we turned to the field of information theory, where concepts such as '*static*' and '*information content*' have explicit mathematical definitions. Specifically, we indirectly measured neural information (i.e., the opposite of static) by computing and contrasting the spatial complexity – using both Lempel-Ziv and Kolmogorov complexity – of the cortical patterns of activation in blood-oxygenation-level-dependent (BOLD) signal in the ventral temporal lobes of aphantasics, hyperphantasics, and age-matched controls during a simple perception and imagery task (Kaspar and Schuster, 1987; Lempel and Ziv, 1976). Briefly, these algorithms quantify the complexity of the spatial pattern of binarized BOLD activation enacted across the cortical surface by compressing binary vectors representing which parcels are (in)active at each Repetition Time (TR; see Fig. 1). During both typical and highly vivid imagery, we would expect the signal-to-noise ratio of activity in the ventral temporal lobes to be sufficiently large, with background noise remaining below and imagery-related activity surpassing the binarization threshold used by these algorithms, resulting in rich patterns of (in)activation at each TR. Since we hypothesise that aphantasics lack the cortical control to suppress background activity during imagery attempts, background activity may also reach above the binarization threshold used by these algorithms in these individuals, resulting in general patterns of (in)activation at each TR that lack the complexity needed to encode visual information.

Therefore, our key prediction was that aphantasics should be incapable of increasing the spatial information content of the pattern of BOLD activity within their temporal lobes during visual imagery. To determine whether this effect was also related to reduced top-down control, we performed a dynamic functional connectivity (dFC) analysis. The key predictions of our hypotheses were that imagery vividness is correlated with the spatial complexity of BOLD activation in the ventral temporal lobes, and that reduced imagery vividness correlated with decoupling between the temporal lobes and higher-order networks. In both cases, we found robust confirmatory evidence for our hypotheses and thus provide evidence that aphantasia can be effectively characterised as an alteration of neural information processing.

2. Methods

2.1. Participants

70 participants completed the study – full recruitment details can be found in Milton et al. (2021). Prior to scanning, participants performed a modified version (see supplementary materials) of the Vividness of Visual Imagery Questionnaire (VVIQ; Marks, 1973): a 16-item questionnaire that measures imagery vividness by asking participants to imagine a scene and then report the vividness of that image on a 5-point Likert scale (1 = "No image at all, you only "know" that you are thinking of an object"; 5 = "Perfectly clear and as vivid as normal vision"). Using this approach, 24 participants were classified as having aphantasia (VVIQ score between 16 and 23/80; mean age 33.71; sd ± 11.3 years; 10 females) and were asked to confirm their condition was congenital, while 20 were classified as controls with midrange imagery (VVIQ score between 55 and 60/80; mean age 34.6 years; s.d. ± 12.78 years; 9 females). 25 participants were classified as having hyperphantasia (VVIQ score between 75 and 80; mean age 35.36 years; s.d. ± 11.10 years; 17 females). After removing participants with missing data, we were left with a total of 21 aphantasics, 17 controls, and 20 hyperphantasics leaving 58 participants in total (for full further exclusion details, see Milton et al., 2021). Ethical approval for the original study was obtained from the University of Exeter Psychology Ethics Committee.

2.2. Functional magnetic resonance imaging and task design

All images were collected using a 1.5 T scanner (*Intera Phillips*). T1-weighted anatomical images (T1w) of the whole head were centred at the anterior commissure at a resolution of 0.9 × 0.9 × 0.9 mm. BOLD fMRI data were obtained using a T2*-weighted single-shot echoplanar (EPI) scanning sequence (temporal resolution [TR] = 3 s, echo time [TE] = 50 ms, resolution 2.88 × 2.88 × 3.6 mm, 38 slices, 90° flip angle) over two separate 17.5 min imaging runs (each with 364 time points). Each run corresponded to a specific stimulus type: either famous faces or places. Forty stimulus images that were successfully recognised by all the participants were selected from a larger dataset. Within each of the

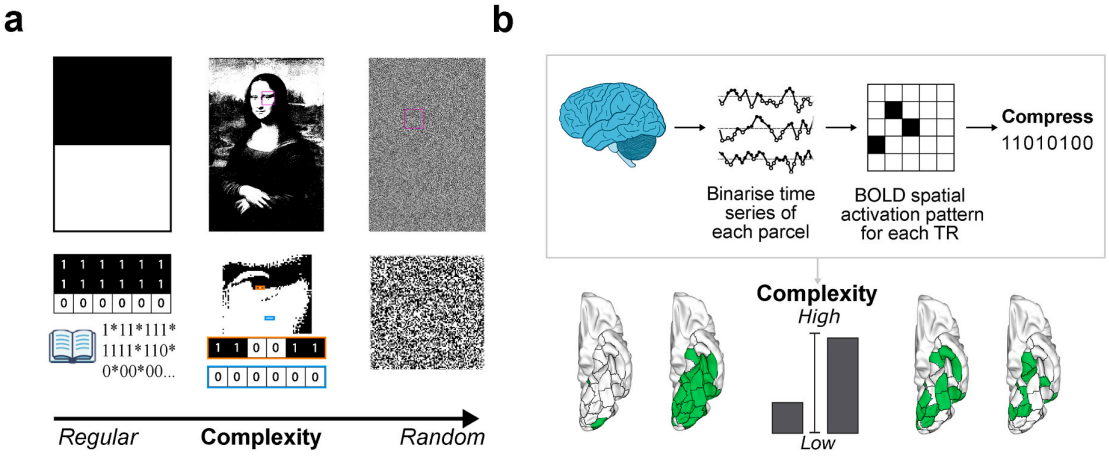

Fig. 1. Complexity (A) Three images arranged in increasing order of spatial complexity (above). If we represent the black and white pixels in the images as 1's and 0's respectively, then LZ76 (i.e. the algorithm that determines Lempel-Ziv complexity) answers the question: "What is the number of entries into a codex needed to store all the binary sequences in the image?". The left-most image is the least complex, consisting of two halves occupied by either repeating 1's or 0's. A graphical depiction of how the LZ76 algorithm calculates the complexity for such sequences is depicted below, highlighting how regular sequences are compressed using previous codex entries. The Mona Lisa (centre) still has many spaces consisting of regular sequences (cyan), but some spaces are more complex (orange), as can be seen in the enlarged portions below. To the right we see that random noise consists of many unique sequences with very few repetitions. (B) Above is the pipeline used to determine spatial complexity of cortical activation. The time series for each brain parcel were binarized, generating a matrix of whether each parcel was "on" or "off" at each repetition time (TR). Vectors for each column of the matrix encoding the spatial patterns of cortical activity at each TR were then compressed by the LZ76 algorithm to quantify the complexity of the spatial pattern. Below the pipeline are two examples of low spatial complexity (left) and high spatial complexity (right) patterns across ventral temporal lobe parcels are depicted. Bar plots are for illustrative purposes. Complexity scores obtained from this pipeline were then fit to general linear models predicting the effects of an imagery and perception task on cortical complexity. (For interpretation of the references to colour in this figure legend, the reader is referred to the Web version of this article.)

runs, the participants performed a block-design task that alternated between perception blocks in which participants viewed images of famous faces or places, calculation blocks (not analysed further here), and an imagery block where they were asked to imagine a famous face or place (for full protocol, see Milton et al., 2021). Each block involved a period in which a stimulus was shown (6 s), followed by a period in which participants used a three-button response pad to answer a presented rating question, and then a blank screen for a randomised duration between 0.5 and 2.5 s. Each block was repeated four times, and the entire sequence of blocks was repeated ten times. During the perception block, participants viewed an image of a face or place and then rated its pleasantness (2 s). During imagery blocks, participants were asked to imagine a previously displayed stimulus. They were then asked to rate the vividness of the image (2 s).

2.3. Preprocessing of anatomical data

The T1w image underwent intensity non-uniformity correction using **N4BiasFieldCorrection** distributed with ANTs 2.3.1 (Avants et al., 2008). The corrected image served as the T1w reference throughout the workflow. Skull-stripping was performed using a *Nipype* implementation of **antsBrainExtraction.sh** workflow with OASIS30ANTs as the target template. Brain tissue segmentation into cerebrospinal fluid, white-matter, and grey-matter was carried out using *FAST* (Zhang et al., 2001).

Volume-based spatial normalization to MNI152NLin6Asym (2 mm) and MNI152NLin2009cAsym templates was achieved through nonlinear registration with **antsRegistration** (ANTs 2.3.1), utilizing brain-extracted versions of both T1w reference and the template. The selected templates were *FSL's MNI ICBM 152 non-linear* 6th *Generation Asymmetric Average Brain Stereotaxic Registration Model* (Zhang et al., 2001) and *ICBM 152 Nonlinear Asymmetrical template version 2009c* (Fonov et al., 2009).

2.4. Preprocessing of functional data

For each of the two BOLD runs per participant, preprocessing included generating a reference volume and its skull-stripped version using a custom *fMRIPrep 21.0.2 methodology* (Esteban et al., 2019). Head-motion parameters were estimated with *mcflirt* (Jenkinson et al., 2002). The BOLD time series were resampled onto their original, native space by applying transforms to correct for head motion. The co-registration of the BOLD reference to the T1w reference involved *MRI_coreg* (FreeSurfer) followed by *FLIRT* (Jenkinson et al., 2002) with the boundary-based registration cost-function (Greve and Fischl, 2009), configured with six degrees of freedom.

Confounding time series, including framewise displacement (FD), DVARS, and three region-wise global signals, were calculated based on the preprocessed BOLD data. Physiological regressors were extracted for component-based noise correction (*CompCor*). Various spatial resamplings generated spatially-normalized, preprocessed BOLD runs in MNI152NLin6Asym and MNI152NLin2009cAsym spaces. All resampling was performed with a single interpolation step by composing all pertinent transformations, including head-motion transform matrices and susceptibility distortion correction when available.

2.5. Software and tools

Many internal operations utilized *Nilearn* 0.9.1 [@nilearn, RRID: SCR_001362] within the functional processing workflow. Additional details about the pipeline can be found in fMRIPrep's documentation (https://fmriprep.org/en/latest/workflows.html).

2.6. Brain parcellation and denoising

Following preprocessing, denoising was performed in *Python* (version 3.7) to remove 12 head-motion-related artefacts and white matter, cerebrospinal fluid noise from the BOLD signal. A band-pass filter was applied (between 0.01 and 0.1 Hz) to remove noise

associated with physiological processes and scanner-related drift. Head-motion distortions were corrected by regressing out 6 head-motion parameters and their corresponding temporal derivatives. Finally, the BOLD time series was z-scored, standardising activity across the whole brain. The mean time series from each of a predefined set of 400 cortical parcels was calculated. These parcels were derived from the 17-Networks Schaefer 400 parcellation scheme (Schaefer et al., 2018; Yeo et al., 2011), which divides the brain into key functional networks including visual and attention networks we deemed important in visual processing. Brain parcels were visualised using the plotSurfaceROIBoundary (v 1.0.1) package in *MATLAB* 9.12.10 (MathWorks; Oldham, 2025).

2.7. Complexity analyses

The spatial complexity of BOLD signal during perception and imagery blocks was calculated from 53 parcels (28 left hemisphere; 25 right hemisphere) corresponding to the anatomical ventral temporal lobes using *MATLAB* 9.12.10 (MathWorks). The BOLD signal from each parcel was binarized to values greater than or less than zero for each TR and then the spatial complexity of the pattern of activation across the parcels at each TR was computed using the 'calc_lz_complexity.m' (Lempel-Ziv complexity; Thai, 2023) and 'kolmogorov.m' (Kolmogorov complexity; Faul, 2023) functions. Note: complexity was not assessed over time (as is typical of previous work; Shine et al., 2019; Medel et al., 2023) but over space, as we were interested in the complexity of the spatial configuration of parcels requiring elevated blood flow during perception and imagery blocks. The effects of the experimental tasks on the observed complexity scores for each participant were estimated using general linear models (GLM) with design matrices constructed by haemodynamically convolving the onset times for each block while they performed the behavioural task (Friston et al., 1994). Given the non-Gaussian nature of the data, Spearman's ρ correlations were calculated to determine the correlation between participants' β-coefficients predicting their complexity score and their VVIQ score. Statistical significance was determined using a non-parametric permutation test in which VVIQ scores were shuffled 5000 times (Nichols and Holmes, 2002). To determine whether the correlation between complexity scores and VVIQ was greater during imagery blocks relative to perception, we subtracted the Spearman's ρ correlation between complexity scores and VVIQ scores during perception from those during imagery and a further permutation test was performed by randomly swapping complexity scores between imagery and perception independently for each participant and recalculating Spearman's ρ correlations 5000 times.

2.8. Standard deviation of BOLD signal in ventral temporal lobes

We computed the standard deviation of BOLD signal in the ventral temporal lobes using the same mask that was used in the complexity analyses (i.e., 53 ventral temporal lobe parcels). The standard deviation was calculated across TRs during the perception blocks and imagery blocks using the onset times for each task. A paired two-tailed *t*-test was performed on the mean standard deviation scores across parcels for each participant during perception and imagery. Next, we calculated the Spearman's correlation coefficient between the mean standard deviations across temporal lobe parcels for each participant and their VVIQ score.

2.9. Dynamic functional connectivity

dFC analysis was conducted in *MATLAB* 9.12.10 (MathWorks) using the multiplication of temporal derivatives (MTD) approach (Shine et al., 2015). The MTD is computed by calculating the point-wise product of the temporal derivatives of pairwise time series (Equation (1)). To reduce contamination of high-frequency noise, the MTD is averaged across a sliding window *w*. MTD scores for each of the 400 parcels was calculated using a sliding temporal window of 10 points (30 s).

$$MTD_{ijt} = \frac{1}{w}\sum_{t}^{t+w}\frac{(dt_{it} \times dt_{jt})}{(\sigma_{dt_i} \times \sigma_{dt_j})} \quad (1)$$

Equation (1). The equation for the pairwise MTD score between parcel i and parcel j at time t, where dt is the temporal derivative of parcel i or j at time t, and σ is the standard deviation of the temporal derivative time series for parcel i or j, and w is the window length of the simple moving average.

A functional connectivity matrix was calculated for each individual time window, resulting in a weighted 3D adjacency matrix (parcel × parcel × time) of MTD scores for each participant. To determine the relationship between the task and MTD scores, GLMs were computed comparing each pairwise MTD score (edge) with each condition using the aforementioned design matrices. Spearman's ρ correlations were calculated, correlating the β-coefficients estimating the edgewise MTD scores for each participant with their VVIQ score, giving a parcel × parcel matrix of ρ values. Significant edges were determined by shuffling participants and recalculating the Spearman's ρ for each edge 5000 times.

A mask was applied to the matrix of ρ values such that only parcels that were deemed statistically significant following permutation testing ($p < 0.05$) were retained. This enabled us to analyse the correlation between dFC – specifically, the connectivity between the functional networks from the Yeo 7-network parcellation scheme with our ventral temporal lobe mask – and participants' VVIQ scores. To assess the contribution of each participant subgroup to these correlations, additional matrices were generated by applying the same mask filtering for significant parcels to the mean β-coefficients estimating MTD scores for aphantasics, controls, and hyperphantasics during imagery, and isolating edges between the Yeo 7-networks and parcels of the ventral temporal lobe mask. Results were visualised using the Circlize Package (version 0.4.16; Gu et al., 2014) in R 4.4.3.

2.10. Univariate analyses

We computed GLMs on BOLD fMRI data during each of the experimental tasks using the aforementioned design matrices (Friston et al., 1994). General linear regression was performed by computing the 'glmfit' function within *MATLAB* 9.12.10 to obtain a set of β-coefficients that estimate the effect of each fMRI task on the observed BOLD signal for each parcel ($n = 502$). For each parcel, we assessed the difference between the β-coefficients for imagery and perception by performing 5000 permutations of the condition labels and computing the mean difference (imagery minus perception) for each permutation.

To identify whether the BOLD activity within any of our 400 cortical parcels was correlated with participants' VVIQ scores, we calculated the Spearman's correlation coefficient between the β-coefficients during imagery and perception of each parcel for each participant and their VVIQ score. Statistical significance was determined using non-parametric permutation tests by shuffling VVIQ scores 5000 times and recomputing the Spearman's correlation coefficient to construct a null distribution.

3. Results

3.1. Complexity

We assessed the relationship between the complexity of the spatial pattern of ventral temporal lobe activity during perception and imagery with participants' VVIQ scores. As seen in Fig. 2A, computing Spearman's correlation coefficients revealed that the β-coefficients predicting Lempel-Ziv complexity in response to the perception task were positively correlated with participants' VVIQ scores ($\rho = 0.171$) and this effect was statistically significant ($p = 0.030$). An even stronger effect

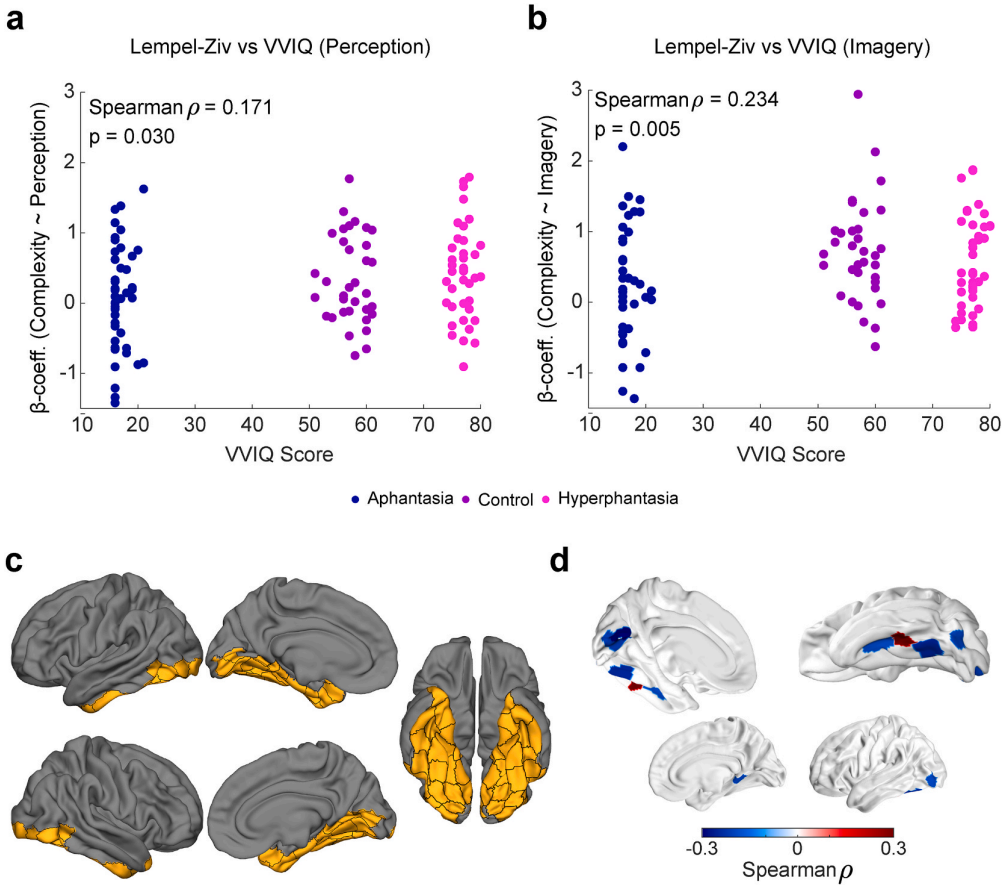

Fig. 2. Lempel-Ziv Complexity and Variance (A) Scatterplot of participants' β-coefficients predicting Lempel-Ziv complexity versus their VVIQ score during perception. Spearman's ρ shows a positive correlation between Lempel-Ziv complexity and VVIQ during perception (ρ = 0.171, p = 0.030). Aphantasics are marked in blue, controls in purple, and hyperphantasics in magenta. (B) Same as (A) but during imagery when an even stronger correlation was observed (ρ = 0.234, p = 0.005). (C) Surface plots showing the 53 parcels included in the ventral temporal lobe mask are outlined in black and shown in yellow. (D) Spearman's ρ correlations between the standard deviation of parcels' signal during imagery and participants' Vividness of Visual Imagery Questionnaire (VVIQ) scores. Only parcels whose correlations were statistically significant ($p < 0.05$) are shown. (For interpretation of the references to colour in this figure legend, the reader is referred to the Web version of this article.)

was observed during imagery (ρ = 0.234, p = 0.005; Fig. 2B).

As a convergent complexity measure, we performed similar comparisons using Kolmogorov complexity. It was observed that the Kolmogorov complexity of ventral temporal lobe activity was positively correlated with VVIQ scores during imagery (ρ = 0.174, p = 0.032; Fig. S1B), while the correlation between Kolmogorov complexity and VVIQ scores during perception was not statistically significant (ρ = 0.092, p = 0.159; Fig. S1A).

Next, we sought to determine whether the observed Spearman's ρ corelations between complexity scores during imagery blocks were stronger relative to perception. There was no statistically significant difference between the Spearman's ρ correlations for complexity and VVIQ scores during imagery and perception blocks for Lempel-Ziv complexity (Δρ = 0.063; p = 0.248) nor Kolmogorov complexity (Δρ = 0.082; p = 0.192).

3.2. Standard deviation of ventral temporal lobe activity

To determine which parcels may be driving reduced complexity in individuals with low VVIQ scores, we investigated the standard deviation of the BOLD signal within the 53 parcels of the ventral temporal lobe mask. A statistically significant difference between parcels' standard deviations during perception and imagery was observed (t (115) = −8.797, $p < 1 \times 10^{-13}$). During perception, only the standard deviation of one parcel within the lingual gyrus of the left hemisphere (Schaefer parcel no. 15) had a statistically significant correlation with VVIQ scores (ρ = −0.215, p = 0.021). During imagery, the standard deviations of several parcels within the left ventral temporal lobe, one in the calcarine sulcus, and one parcel at the isthmus of the cingulate gyrus in the right hemisphere had statistically significant correlations with VVIQ scores ($p < 0.05$; Table S1 and Fig. 2D).

3.3. Dynamic functional connectivity

Fig. 3 depicts the Spearman's correlation coefficient between participants' VVIQ scores and β-coefficients predicting MTD scores between the Yeo 7-networks and the ventral temporal lobes. Only statistically significant correlations are depicted ($p < 0.05$). The mean MTD score contribution of each subgroup to the correlations in Fig. 3 (i.e. aphantasia, control, hyperphantasia) is depicted in Fig. S2. Many parcels within the left frontoparietal, left default mode, right dorsal attention, right motor, and right visual networks were anticorrelated with VVIQ scores. The Yeo 7-networks that contained many parcels whose dFC with the ventral temporal lobes was positively correlated with VVIQ scores included the left ventral attention, the frontotemporal, and the frontoparietal networks with the bilateral temporal lobes, as well as the right

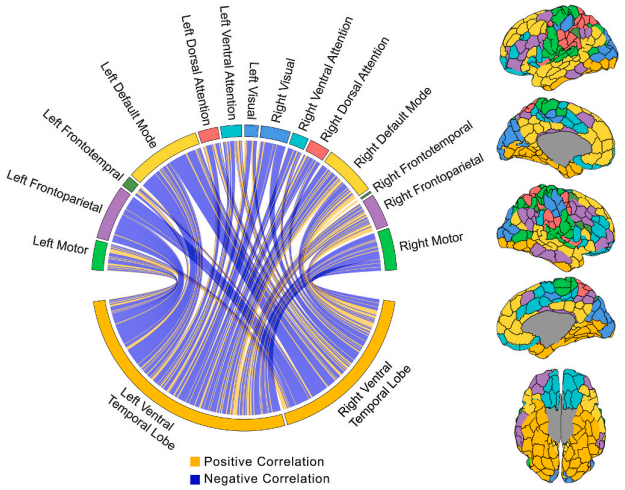

Fig. 3. Correlation between VVIQ and the Dynamic Functional Connectivity between Schaefer Networks and the Ventral Temporal Lobes Chord plot showing Spearman's correlation coefficients between participants' Vividness of Visual Imagery Questionnaire (VVIQ) scores and β-coefficients predicting multiplication of temporal derivatives (MTD) scores. Correlations are calculated between the Yeo 7-networks (cortical maps on the right) and parcels within a predefined ventral temporal lobe mask (53 parcels) during imagery. Positive edges (yellow) show a positive correlation between MTD score and VVIQ and vice versa for blue edges. The connections' thickness is proportional to the strength of the correlation (i.e., thicker connections indicate greater increase/decrease and vice versa). Only parcels with statistically significant correlations between MTD scores and VVIQ are shown ($p < 0.05$). (For interpretation of the references to colour in this figure legend, the reader is referred to the Web version of this article.)

default mode network with the right temporal lobe, and the left motor network with the right temporal lobe. It was observed that edges that showed positive correlations with VVIQ scores corresponded to edges with increased connectivity in hyperphantasics and controls relative to aphantasics, whilst edges with increased connectivity in aphantasics typically corresponded to edges that were negatively correlated with VVIQ scores (Fig. S2).

3.4. Univariate analyses

We performed univariate analyses to determine whether there were any differences in global BOLD activation during perception and imagery, and to examine whether global BOLD activity was correlated with participants' VVIQ scores. First, we observed changes in BOLD activation associated with perception across all participants. Activation showed a gradient of decreasing activation starting in the primary visual cortices—which showed markedly increased activation—and ending in the frontal cortices which showed relatively less activation compared to resting activity, however, some parcels of the prefrontal cortex also showed slightly increased activity (Fig. S3C). Next, we determined whether the activity of any parcels during imagery differed from perception by computing the mean difference of BOLD activity (imagery minus perception). Fig. S3D and Table S2 show parcels considered to have statistically significantly different activity during imagery relative to perception ($p < 0.05$). Overall, it was observed that there was less activity in the primary visual cortices during imagery relative to perception. In contrast, increased activity distributed throughout parcels of the left hemisphere, particularly parcels of the prefrontal and parietal cortices corresponding to parcels of the dorsal attention and ventral attention networks, as well as parcels of the superior temporal gyrus.

To determine whether the BOLD activity of parcels was correlated with participants' VVIQ scores, we calculated the Spearman's correlation coefficient between the β-coefficient predicting each parcel's BOLD activity during imagery and perception for each participant and their VVIQ score. Fig. S3A and Table S3 show the statistically significant Spearman's correlation coefficients ($p < 0.05$) between BOLD activity during perception and VVIQ scores, while Fig. S3B and Table S4 depict similar results but during imagery instead. It was observed in both cases that parcels of the right frontal cortices were anticorrelated with VVIQ scores.

4. Discussion

In this study, we performed a novel analysis of fMRI data collected in a previous experiment to test the hypothesis that individuals with aphantasia experience a poverty of visual imagery due to an inability to voluntarily differentiate neural signals within their ventral temporal lobes. Accordingly, we observed a positive correlation between the spatial complexity of BOLD activity in the ventral temporal lobes and participants' VVIQ scores (Fig. 2 and Fig. S1). Additionally, key higher-order functional networks of aphantasics were abnormally coupled with the ventral temporal lobes (Fig. 3 and Fig. S2), with decreased connectivity between many parcels whose connectivity were shown to be correlated with VVIQ scores and vice versa. Importantly, we present a novel quantification of the abnormal information processing inherent within the brains of individuals with aphantasia. We suggest future research should investigate the underlying neural mechanisms might be, keeping in mind aphantasia likely arises due to multiple neurological factors (Dawes et al., 2024; Spagna et al., 2021).

To our knowledge, this is the first study to quantify information content as a proxy for imagery vividness. Although exploratory and requiring replication in larger samples, this finding is promising in that it aligns with the intuition that more vivid imagery would require more visual information to be processed in higher-order visual regions. If this is indeed the case, then aphantasia may be the result of an "information lesion" in the ventral temporal lobes. Interestingly, we also observed Lempel-Ziv complexity—but not Kolmogorov complexity—was correlated with vividness during perception. While the correlations between complexity and perception were less than imagery, the difference between the complexities during both tasks was not statistically significant for either measure. Our initial prediction was that complexity differences would be present during imagery only. Although this result may be due to excess noise in the current dataset, it also highlights that we cannot yet determine whether 'normal' perception is impaired in individuals with aphantasia – i.e., perception could be practically fine, but distinct for non-aphantasics. It is our hope that further applications of spatial complexity analyses may illuminate questions concerning atypical imagery, such as whether the heterogeneity of aphantasia can be explained by varying profiles of information loss, or if and how other regions contribute to imagery vividness.

For instance, while the current study focused on complexity in the ventral temporal lobes, it remains unclear whether activity in the primary visual cortices is necessary or sufficient for imagery (Milton, 2024; Spagna et al., 2021). The contents of V1 have been decoded by recent studies using multivariate pattern analysis from aphantasics during imagery and while they listened to auditory stimuli. This suggests that such activity may not be closely tied to the subjective experience of imagery (Cabbai et al., 2024; Chang et al., 2025; Montabes de la Cruz et al., 2024). However, multivariate pattern analysis can only confirm the presence of decodable patterns of activation and is not sensitive enough to probe the underlying richness of this activity. Instead, by implementing information-theoretic approaches such as those used in the current study, it may be possible to quantify the richness of information content at various stages of the visual processing hierarchy, regardless of overall BOLD activation or decodability.

Given the exploratory nature of our study and that the spatial resolution of our dataset was relatively low, we analysed spatial complexity

at the region-level to maximise the chance of detecting an effect. A finer-grained analysis, ideally using a higher spatial resolution dataset than the current study's to minimise noise, would enable quantification of information between and within different parcels of the visual processing hierarchy. Such an analysis may prove to be more sensitive to detecting variations in imagery vividness. Doing so may also help determine whether imagery vividness is underpinned by different levels of complexity at different scales, different cortical layers, or whether excess noise is generated from a lack of sensory suppression where functionally segregated regions for perception and imagery overlap (Anderson et al., 2025; Carricarte et al., 2024, 2025). Therefore, we hope future studies seek to reproduce and expand our initial findings across different scales.

Our initial hypothesis – informed by findings from Keogh et al. (2020) – was that hyperexcitability within visual processing regions produces excess noise, preventing sufficient and specific activation in these regions above background levels of activity. We analysed the relationship between the standard deviation of signals within the ventral temporal lobes during imagery with participants' reported imagery vividness. Regions with higher variance have more opportunity to differentiate, leading to an increase in complexity and vice versa. While the variance of signal from several regions was negatively correlated with vividness, higher signal variation of a particular parcel in the ventral temporal lobe was associated with increased vividness. This parcel is spatially contiguous with a region that has been previously identified as a key hub during mental imagery: the fusiform imagery node (Liu et al., 2025; Spagna et al., 2021). This may suggest that imagery vividness is determined by increased information driven by a high variation in the activity of the fusiform imagery node, as well as the suppression of noise from surrounding regions. However, these findings remain speculative and our results on their own cannot speak to the role of hyperexcitability or any other mechanism in determining imagery vividness. Further research is needed to identify differences in the micro- and mesoscale circuitry that determine signal-to-noise during imagery.

We also hypothesized that reduced imagery vividness was accompanied by decoupling between higher-order networks and the ventral temporal lobes. Analysing the correlation of the dFC between the Yeo 7-networks and the temporal lobes with VVIQ scores revealed that positive correlations were related to greater decoupling between higher-order networks and the ventral temporal lobes in aphantasics, while positive edges in aphantasia tended to contribute to anticorrelations with VVIQ. It should be noted that within the 'aphantasia' group we have included individuals with both minimal and low vividness according to their VVIQ responses, and as such our results may not be consistent with those of individuals with absent imagery (Blomkvist and Marks, 2023; Purkart et al., 2025). Relatively few positive connections in controls and hyperphantasics contributed to the profile of significant correlations between dFC and VVIQ compared to the numerous negative connections. We hypothesise that this likely reflects that controls and hyperphantasics are better able to suppress irrelevant communication and selectively engage nodes within their imagery networks.

Reduced vividness appears to be driven by decoupling between the ventral attention and dorsal attention networks with the bilateral temporal lobes of aphantasics. The dorsal attention network is important for exogenous, voluntary attention, while the ventral attention network plays an important role in switching the brain between endogenous and exogenous states of attention, as well as in orientating attention toward salient stimuli (Ghosh et al., 2019; Shine et al., 2011). The ventral attention network is also right hemisphere dominant, and we observed that reduced imagery vividness is driven by greater decoupling between the right ventral attention network and the bilateral temporal lobes of aphantasics accordingly (Corbetta et al., 2008). Both the ventral attention and dorsal attention networks occupy frontoparietal regions as well as regions within the temporal and medial association cortices (Corbetta and Shulman, 2002; Tosoni et al., 2023). It has been previously shown that during imagery, inputs from frontoparietal regions involved in attention and working memory act to maintain the image in conscious awareness after information from long-term memory has been retrieved (Fulford et al., 2018; Spagna et al., 2021). Therefore, these networks are key to orchestrating visuospatial attention and play an extensive role in both perception and imagery, and decoupling of the ventral and dorsal attention networks with the temporal lobes appears to disrupt the brain's ability to maintain the vividness of an internally generated image.

The dFC between the default mode network and temporal lobes appears to have a complex relationship with imagery vividness, which is reflected by current speculations concerning the role of the default mode network in imagery generation. The default mode network is well-known for being active during self-generated mental states such as working memory, dreaming, theory of mind, and thinking about the future (Aichhorn et al., 2003; Andrews-Hanna et al., 2014; Fox et al., 2013; Menon, 2023; Spreng et al., 2009). Increased default mode activity and connectivity has been previously shown to increase imagery vividness (Fulford et al., 2018; Spagna et al., 2021), while decoupling of the default mode plays a role in psychedelic experiences (Carhart-Harris et al., 2012; De Araujo et al., 2012; Gattuso et al., 2023). We hypothesise that positive edges between the default mode network and the temporal lobes of aphantasics may simply indicate that the brain is not engaged in mental imagery and is "mind wandering", while the specific positive edges in controls and hyperphantasics may contribute to imagery generation. However, evidence suggests that sub-networks of the default mode require precision fMRI performed using a 7 T scanner to be fully resolved (Braga et al., 2019; Braga and Buckner, 2017; DiNicola et al., 2023; Du et al., 2024). Since we used 1.5 T fMRI data and performed a group-level analysis, it is possible we cannot draw sufficient conclusions, and further research is needed to capture nuanced differences caused by anatomical variation between participants and correctly determine the role of the default mode network in imagery vividness.

Our results constitute the first dFC analysis in an aphantasic cohort, building upon previous fMRI studies of aphantasia which have primarily used static functional connectivity, univariate, and multivariate analyses of BOLD signals. While such analyses have their place, they assume stationarity of the BOLD signal and risk mischaracterising the underlying mechanisms of imagery vividness and aphantasia. Therefore, dFC is able to shed new insight into the inherently dynamic processes of imagery and perception, but the approach used in the current study is not without its own limitations. For instance, we analysed dFC between group-level network masks, which may introduce imprecision at the boundaries of functional networks given anatomical variations between participants. Also, subcortical analyses were not performed in the current study as the low spatial resolution of our dataset was insufficient to resolve subcortical structures. Existing evidence shows there is more insight to be gained by analysing subcortical dFC. Monzel et al. (2024) found that the static functional connectivity between the hippocampus and primary visual regions of controls showed a strong negative correlation when compared to aphantasics, which they suggest may reflect a lack of inhibition of sensory noise that impairs imagery generation. Therefore, we suggest future studies expand our dFC approach to conduct a more comprehensive, whole brain dFC analysis including subcortical regions.

We also performed a series of univariate analyses, in which we were able to successfully recreate canonical activation patterns during perception and imagery, as well as recreate results published in more recent findings. During imagery, we observed that there is greater activation of regions in the ventral attention and dorsal attention networks of the left hemisphere, which agrees with current theories that imagery tends to be lateralised (Spagna et al., 2021). Furthermore, we found activity in regions of the right ventral and dorsal attention networks were negatively correlated with imagery vividness, supporting recent findings from Liu et al. (2025) that aphantasics show increased activity in regions of the right ventral attention network.

In summary, the current study investigated the dFC and spatial complexity differences underlying imagery vividness. We observed that the spatial complexity of BOLD activity in the ventral temporal lobes is correlated with imagery vividness. We also observed that decreased vividness is associated with decreased connectivity between the temporal lobes and frontoparietal networks including the dorsal attention and ventral attention networks in aphantasia. Our results provide a novel way of understanding aphantasia as an information lesion, which we speculate is due to excess noise preventing the ventral temporal lobes from differentiating signals encoding visual stimuli above background levels of activity, as well as decreased and less specific input from high-order brain regions, which we hope will form the basis of future studies.

CRediT authorship contribution statement

Chanelle Noble: Writing – review & editing, Writing – original draft, Visualization, Formal analysis. **Natasha L. Taylor:** Writing – review & editing, Formal analysis. **Fraser Milton:** Writing – review & editing, Data curation. **Jon Fulford:** Data curation. **Joshua B. Tan:** Writing – review & editing, Formal analysis. **Claire O'Callaghan:** Writing – review & editing. **Adam Zeman:** Writing – review & editing, Conceptualization. **James M. Shine:** Writing – review & editing, Supervision, Methodology, Formal analysis, Conceptualization.

Code availability

Deidentified, preprocessed time series data and all code used to analyse the data in this study is available from https://github.com/chanellenoble/Aphantasia_complexity.

Funding

The funding for the current study was provided by the National Health and Medical Research Council (NHMRC GNT1193857) and Australian Research Council (ARC DP240101295). The original study by Milton et al. (2021) was supported by funding from the United Kingdom Arts and Humanities Research Council Science in Culture Innovation Award: The Eye's Mind—a study of the neural basis of visual imagination and its role in culture (AH/M002756/1); Follow-on Funding Award: Extreme Imagination in Mind, Brain and Culture (AH/R004684/1).

Acknowledgements

The authors acknowledge the Sydney Informatics Hub and the use of the University of Sydney's high performance computing cluster, Artemis.

Appendix A. Supplementary data

Supplementary data to this article can be found online at https://doi.org/10.1016/j.neuropsychologia.2025.109322.

References

Aichhorn, M., Perner, J., Kronbichler, M., Staffen, W., Ladurner, G., Berthoz, S., Armony, J., Blair, R., Dolan, R., Blakemore, S., 2003. People thinking about thinking people: the role of the temporo-parietal junction in "theory of mind". Neuroimage 19, 1835–1842.

Anderson, N.L., Salvo, J.J., Smallwood, J., Braga, R.M., 2025. Distinct distributed brain networks dissociate self-generated mental states. bioRxiv 2025 (2002), 640604, 2027.

Andrews-Hanna, J.R., Saxe, R., Yarkoni, T., 2014. Contributions of episodic retrieval and mentalizing to autobiographical thought: evidence from functional neuroimaging, resting-state connectivity, and fMRI meta-analyses. Neuroimage 91, 324–335.

Avants, B.B., Epstein, C.L., Grossman, M., Gee, J.C., 2008. Symmetric diffeomorphic image registration with cross-correlation: evaluating automated labeling of elderly and neurodegenerative brain. Med. Image Anal. 12 (1), 26–41.

Blomkvist, A., Marks, D.F., 2023. Defining and 'diagnosing'aphantasia: condition or individual difference? Cortex 169, 220–234.

Braga, R.M., Buckner, R.L., 2017. Parallel interdigitated distributed networks within the individual estimated by intrinsic functional connectivity. Neuron 95 (2), 457–471. e455.

Braga, R.M., Van Dijk, K.R., Polimeni, J.R., Eldaief, M.C., Buckner, R.L., 2019. Parallel distributed networks resolved at high resolution reveal close juxtaposition of distinct regions. J. Neurophysiol. 121 (4), 1513–1534.

Cabbai, G., Racey, C., Simner, J., Dance, C., Ward, J., Forster, S., 2024. Sensory representations in primary visual cortex are not sufficient for subjective imagery. Curr. Biol. 34 (21), 5073–5082.e5075. https://doi.org/10.1016/j.cub.2024.09.062.

Carhart-Harris, R.L., Erritzoe, D., Williams, T., Stone, J.M., Reed, L.J., Colasanti, A., Tyacke, R.J., Leech, R., Malizia, A.L., Murphy, K., 2012. Neural correlates of the psychedelic state as determined by fMRI studies with psilocybin. Proc. Natl. Acad. Sci. 109 (6), 2138–2143.

Carricarte, T., Iamshchinina, P., Trampel, R., Chaimow, D., Weiskopf, N., Cichy, R.M., 2024. Laminar dissociation of feedforward and feedback in high-level ventral visual cortex during imagery and perception. iScience 27 (7).

Carricarte, T., Xie, S., Singer, J., Trampel, R., Huber, L., Weiskopf, N., Cichy, R.M., 2025. Layer-specific spatiotemporal dynamics of feedforward and feedback in human visual object perception. bioRxiv 2025, 2005. 2013.653501.

Chang, S., Zhang, X., Cao, Y., Pearson, J., Meng, M., 2025. Imageless imagery in aphantasia revealed by early visual cortex decoding. Curr. Biol. 35 (3), 591–599. e594.

Corbetta, M., Patel, G., Shulman, G.L., 2008. The reorienting system of the human brain: from environment to theory of mind. Neuron 58 (3), 306–324.

Corbetta, M., Shulman, G.L., 2002. Control of goal-directed and stimulus-driven attention in the brain. Nat. Rev. Neurosci. 3 (3), 201–215. https://doi.org/10.1038/nrn755 [Article].

Dance, C.J., Ipser, A., Simner, J., 2022. The prevalence of aphantasia (imagery weakness) in the general population. Conscious. Cognit. 97, 103243. https://doi.org/10.1016/j.concog.2021.103243.

Dawes, A.J., Keogh, R., Andrillon, T., Pearson, J., 2020. A cognitive profile of multi-sensory imagery, memory and dreaming in aphantasia. Sci. Rep. 10 (1), 10022. https://doi.org/10.1038/s41598-020-65705-7.

Dawes, A.J., Keogh, R., Pearson, J., 2023. Multisensory subtypes of aphantasia: mental imagery as supramodal perception in reverse. Neurosci 201, 50–59.

Dawes, A.J., Keogh, R., Pearson, J., 2024. Multisensory subtypes of aphantasia: mental imagery as supramodal perception in reverse. Neurosci. Res. 201, 50–59.

De Araujo, D.B., Ribeiro, S., Cecchi, G.A., Carvalho, F.M., Sanchez, T.A., Pinto, J.P., de Martinis, B.S., Crippa, J.A., Hallak, J.E., Santos, A.C., 2012. Seeing with the eyes shut: neural basis of enhanced imagery following ayahuasca ingestion. Hum. Brain Mapp. 33 (11), 2550–2560.

Dijkstra, N., Ambrogioni, L., Vidaurre, D., van Gerven, M., 2020. Neural dynamics of perceptual inference and its reversal during imagery. eLife 9, e53588.

Dijkstra, N., Bosch, S.E., van Gerven, M.A., 2019. Shared neural mechanisms of visual perception and imagery. Trends Cognit. Sci. 23 (5), 423–434.

Dijkstra, N., Mostert, P., Lange, F.P.d., Bosch, S., van Gerven, M.A., 2018. Differential temporal dynamics during visual imagery and perception. eLife 7, e33904.

DiNicola, L.M., Ariyo, O.I., Buckner, R.L., 2023. Functional specialization of parallel distributed networks revealed by analysis of trial-to-trial variation in processing demands. J. Neurophysiol. 129 (1), 17–40.

Du, J., DiNicola, L.M., Angeli, P.A., Saadon-Grosman, N., Sun, W., Kaiser, S., Ladopoulou, J., Xue, A., Yeo, B.T., Eldaief, M.C., 2024. Organization of the human cerebral cortex estimated within individuals: networks, global topography, and function. J. Neurophysiol. 131 (6), 1014–1082.

Esteban, O., Markiewicz, C.J., Blair, R.W., Moodie, C.A., Isik, A.I., Erramuzpe, A., Kent, J. D., Goncalves, M., DuPre, E., Snyder, M., 2019. fMRIPrep: a robust preprocessing pipeline for functional MRI. Nat. Methods 16 (1), 111–116.

Faul, S., 2023. Kolmogorov complexity. MATLAB Central File Exchange. Retrieved November 6, 2023 from. https://au.mathworks.com/matlabcentral/fileexchange/6886-kolmogorov-complexity.

Fonov, V.S., Evans, A.C., McKinstry, R.C., Almli, C.R., Collins, D., 2009. Unbiased nonlinear average age-appropriate brain templates from birth to adulthood. Neuroimage 47, S102.

Fox, K.C., Nijeboer, S., Solomonova, E., Domhoff, G.W., Christoff, K., 2013. Dreaming as mind wandering: evidence from functional neuroimaging and first-person content reports. Front. Hum. Neurosci. 7, 412.

Friston, K.J., Holmes, A.P., Worsley, K.J., Poline, J.P., Frith, C.D., Frackowiak, R.S., 1994. Statistical parametric maps in functional imaging: a general linear approach. Hum. Brain Mapp. 2 (4), 189–210.

Fulford, J., Milton, F., Salas, D., Smith, A., Simler, A., Winlove, C., Zeman, A., 2018. The neural correlates of visual imagery vividness - an fMRI study and literature review. Cortex 105, 26–40. https://doi.org/10.1016/j.cortex.2017.09.014.

Gattuso, J.J., Perkins, D., Ruffell, S., Lawrence, A.J., Hoyer, D., Jacobson, L.H., Timmermann, C., Castle, D., Rossell, S.L., Downey, L.A., 2023. Default mode network modulation by psychedelics: a systematic review. Int. J. Neuropsychopharmacol. 26 (3), 155–188.

Ghosh, P., Roy, D., Banerjee, A., 2019. Characterization of Neural Communication Dynamics in the Ventral Attention Network Across Distinct Spatial and spatio-temporal Scales.

Greve, D.N., Fischl, B., 2009. Accurate and robust brain image alignment using boundary-based registration. Neuroimage 48 (1), 63–72.

Gu, Z., Gu, L., Eils, R., Schlesner, M., Brors, B., 2014. Circlize implements and enhances circular visualization in R. Bioinformatics 30 (19), 2811–2812. https://doi.org/10.1093/bioinformatics/btu393. Epub 2014 Jun 14. PMID: 24930139.

Horikawa, T., Kamitani, Y., 2017. Generic decoding of seen and imagined objects using hierarchical visual features. Nat. Commun. 8 (1), 15037.

Huang, J.Y., Wang, C., Dreher, B., 2017. Silencing "top-down" cortical signals affects spike-responses of neurons in cat's "intermediate" visual cortex. Front. Neural Circ. 11, 27.
Hupé, J., James, A., Payne, B., Lomber, S., Girard, P., Bullier, J., 1998. Cortical feedback improves discrimination between figure and background by V1, V2 and V3 neurons. Nature 394 (6695), 784–787.
Ishai, A., Haxby, J.V., Ungerleider, L.G., 2002. Visual imagery of famous faces: effects of memory and attention revealed by fMRI. Neuroimage 17 (4), 1729–1741.
Ishai, A., Ungerleider, L.G., Haxby, J.V., 2000. Distributed neural systems for the generation of visual images. Neuron 28 (3), 979–990.
Jenkinson, M., Bannister, P., Brady, M., Smith, S., 2002. Improved optimization for the robust and accurate linear registration and motion correction of brain images. Neuroimage 17 (2), 825–841.
Kaspar, F., Schuster, H., 1987. Easily calculable measure for the complexity of spatiotemporal patterns. Phys. Rev. 36 (2), 842.
Kay, L., Keogh, R., Andrillon, T., Pearson, J., 2022. The pupillary light response as a physiological index of aphantasia, sensory and phenomenological imagery strength. eLife 11. https://doi.org/10.7554/eLife.72484.
Keogh, R., Bergmann, J., Pearson, J., 2020. Cortical excitability controls the strength of mental imagery. eLife 9, e50232.
Keogh, R., Pearson, J., 2018. The blind mind: no sensory visual imagery in aphantasia. Cortex 105, 53–60.
Keogh, R., Pearson, J., 2024. Revisiting the blind mind: still no evidence for sensory visual imagery in individuals with aphantasia. Neurosci. Res. 201, 27–30.
Keogh, R., Wicken, M., Pearson, J., 2021. Visual working memory in aphantasia: retained accuracy and capacity with a different strategy. Cortex 143, 237–253. https://doi.org/10.1016/j.cortex.2021.07.012.
Lee, S.-H., Kravitz, D.J., Baker, C.I., 2012. Disentangling visual imagery and perception of real-world objects. Neuroimage 59 (4), 4064–4073.
Lempel, A., Ziv, J., 1976. On the complexity of finite sequences. IEEE Trans. Inf. Theor. 22 (1), 75–81.
Liu, J., Zhan, M., Hajhajate, D., Spagna, A., Dehaene, S., Cohen, L., Bartolomeo, P., 2025. Visual mental imagery in typical imagers and in aphantasia: a millimeter-scale 7-T fMRI study. Cortex 185, 113–132.
Mantegna, F., Olivetti, E., Schwedhelm, P., Baldauf, D., 2025. Covariance-based decoding reveals content-specific feature integration and top-down processing for imagined faces versus places. NeuroImage 331, 121171.
Marks, D.F., 1973. Visual imagery differences in the recall of pictures. Br J Psychol 64 (1), 17–24.
Mechelli, A., Price, C.J., Friston, K.J., Ishai, A., 2004. Where bottom-up meets top-down: neuronal interactions during perception and imagery. Cerebr. Cortex 14 (11), 1256–1265.
Medel, V., Irani, M., Crossley, N., Ossandón, T., Boncompte, G., 2023. Complexity and 1/f slope jointly reflect brain states. Sci. Rep. 13 (1), 21700.
Menon, V., 2023. 20 years of the default mode network: a review and synthesis. Neuron 111 (16), 2469–2487.
Milton, F., 2024. Mental imagery: the role of primary visual cortex in aphantasia. Curr. Biol. 34 (21), R1088–R1090.
Milton, F., Fulford, J., Dance, C., Gaddum, J., Heuerman-Williamson, B., Jones, K., Knight, K.F., MacKisack, M., Winlove, C., Zeman, A., 2021. Behavioral and neural signatures of visual imagery vividness extremes: aphantasia versus hyperphantasia. Cereb Cortex Commun 2 (2), 035. https://doi.org/10.1093/texcom/tgab035.
Montabes de la Cruz, B.M., Abbatecola, C., Luciani, R.S., Paton, A.T., Bergmann, J., Vetter, P., Petro, L.S., Muckli, L.F., 2024. Decoding sound content in the early visual cortex of aphantasic participants. Curr. Biol. 34 (21), 5083–5089.e5083. https://doi.org/10.1016/j.cub.2024.09.008.
Monzel, M., Leelaarporn, P., Lutz, T., Schultz, J., Brunheim, S., Reuter, M., McCormick, C., 2024. Hippocampal-occipital connectivity reflects autobiographical memory deficits in aphantasia. eLife 13, 94916.
Monzel, M., Mitchell, D., Macpherson, F., Pearson, J., Zeman, A., 2022. Proposal for a consistent definition of aphantasia and hyperphantasia: a response to lambert and sibley (2022) and simner and dance (2022). Cortex 152, 74–76. https://doi.org/10.1016/j.cortex.2022.04.003.
Nichols, T.E., Holmes, A.P., 2002. Nonparametric permutation tests for functional neuroimaging: a primer with examples. Hum. Brain Mapp. 15 (1), 1–25.
O'Craven, K.M., Kanwisher, N., 2000. Mental imagery of faces and places activates corresponding stimulus-specific brain regions. J. Cognit. Neurosci. 12 (6), 1013–1023.
Oldham, S., 2025. plotSurfaceROIBoundary: Plot region boundaries on a surface (https://github.com/StuartJO/plotSurfaceROIBoundary/releases/tag/v1.0.1), GitHub. Retrieved November 23, 2025.
Pace, T., Koenig-Robert, R., Pearson, J., 2023. Different mechanisms for supporting mental imagery and perceptual representations: modulation versus excitation. Psychol. Sci., 09567976231198435
Pearson, J., 2019. The human imagination: the cognitive neuroscience of visual mental imagery. Nat. Rev. Neurosci. 20 (10), 624–634. https://doi.org/10.1038/s41583-019-0202-9.
Purkart, R., Delem, M., Ranson, V., Andrey, C., Versace, R., Cavalli, E., Plancher, G., 2025. Are there unconscious visual images in aphantasia? Development of an implicit priming paradigm. Cognition 256, 106059.
Schaefer, A., Kong, R., Gordon, E.M., Laumann, T.O., Zuo, X.-N., Holmes, A.J., Eickhoff, S.B., Yeo, B.T., 2018. Local-global parcellation of the human cerebral cortex from intrinsic functional connectivity MRI. Cerebr. Cortex 28 (9), 3095–3114.
Shine, J.M., Halliday, G.M., Naismith, S.L., Lewis, S.J., 2011. In: Visual Misperceptions and Hallucinations in Parkinson's disease: Dysfunction of Attentional Control Networks?, vol. 26. Wiley Online Library, pp. 2154–2159.
Shine, J.M., Koyejo, O., Bell, P.T., Gorgolewski, K.J., Gilat, M., Poldrack, R.A., 2015. Estimation of dynamic functional connectivity using multiplication of temporal derivatives. Neuroimage 122, 399–407.
Shine, J.M., Breakspear, M., Bell, P.T., Ehgoetz Martens, K.A., Shine, R., Koyejo, O., Sporns, O., Poldrack, R.A., 2019. Human cognition involves the dynamic integration of neural activity and neuromodulatory systems. Nat. Neurosci. 22 (2), 289–296.
Spagna, A., Hajhajate, D., Liu, J., Bartolomeo, P., 2021. Visual mental imagery engages the left fusiform gyrus, but not the early visual cortex: a meta-analysis of neuroimaging evidence. Neurosci. Biobehav. Rev. 122, 201–217. https://doi.org/10.1016/j.neubiorev.2020.12.029.
Spagna, A., Heidenry, Z., Miselevich, M., Lambert, C., Eisenstadt, B.E., Tremblay, L., Liu, Z., Liu, J., Bartolomeo, P., 2024. Visual mental imagery: evidence for a heterarchical neural architecture. Phys. Life Rev. 48, 113–131. https://doi.org/10.1016/j.plrev.2023.12.012.
Spreng, R.N., Mar, R.A., Kim, A.S.N., 2009. The common neural basis of autobiographical memory, prospection, navigation, theory of mind, and the default mode: a quantitative meta-analysis. J. Cognit. Neurosci. 21 (3), 489–510. https://doi.org/10.1162/jocn.2008.21029.
Thai, Q., 2023. Calc_lz_complexity. from. https://au.mathworks.com/matlabcentral/fileexchange/38211-calc_lz_complexity. (Accessed 20 October 2023).
Tosoni, A., Capotosto, P., Baldassarre, A., Spadone, S., Sestieri, C., 2023. Neuroimaging evidence supporting a dual-network architecture for the control of visuospatial attention in the human brain: a mini review. Front. Hum. Neurosci. 17, 1250096.
VanRullen, R., Reddy, L., 2019. Reconstructing faces from fMRI patterns using deep generative neural networks. Commun. Biol. 2 (1), 193. https://doi.org/10.1038/s42003-019-0438-y.
Wicken, M., Keogh, R., Pearson, J., 2021. The critical role of mental imagery in human emotion: insights from fear-based imagery and aphantasia. Proc. Biol. Sci. 288 (1946), 20210267. https://doi.org/10.1098/rspb.2021.0267.
Winlove, C.I., Milton, F., Ranson, J., Fulford, J., MacKisack, M., Macpherson, F., Zeman, A., 2018. The neural correlates of visual imagery: a co-ordinate-based meta-analysis. Cortex 105, 4–25.
Yeo, B.T., Krienen, F.M., Sepulcre, J., Sabuncu, M.R., Lashkari, D., Hollinshead, M., Roffman, J.L., Smoller, J.W., Zöllei, L., Polimeni, J.R., Fischl, B., Liu, H., Buckner, R. L., 2011. The organization of the human cerebral cortex estimated by intrinsic functional connectivity. J. Neurophysiol. 106 (3), 1125–1165. https://doi.org/10.1152/jn.00338.2011.
Zeman, A., 2024. Aphantasia and hyperphantasia: exploring imagery vividness extremes. Trends Cognit. Sci. 28, 467–480.
Zeman, A.Z., Della Sala, S., Torrens, L.A., Gountouna, V.-E., McGonigle, D.J., Logie, R.H., 2010. Loss of imagery phenomenology with intact visuo-spatial task performance: a case of 'blind imagination'. Neuropsychologia 48 (1), 145–155.
Zeman, A.Z., Dewar, M., Della Sala, S., 2015. Lives Without imagery-congenital Aphantasia.
Zhang, Y., Brady, M., Smith, S., 2001. Segmentation of brain MR images through a hidden markov random field model and the expectation-maximization algorithm. IEEE Trans. Med. Imag. 20 (1), 45–57. https://doi.org/10.1109/42.906424.